scientific reports

Check for updates

OPEN

Synthesis of iron oxide/activated hydrochar composite from residual brewery biomass for remediation of water contaminated with chlorophenol

Matías Kopp[1], Pedro Anabalón[1], Sebastián Rocha[3], María Eugenia González[2], Juan Miguel Romero-García[4], Eulogio Castro[4] & Mara Cea[2]✉

This study presents the development of iron oxide/activated hydrochar composites from brewer's spent grain (BSG) to remove 2-chlorophenol (2-CP) from water via adsorption and Fenton oxidation. Two synthesis methods were employed: (1) incipient wetness impregnation via hydrothermal carbonization (FeOHC) and (2) chemical coprecipitation of iron oxide onto the hydrochar surface (FeOHC-C). Characterization revealed mesoporous structures with surface areas ranging from 44 to 66 $m^2 g^{-1}$ and magnetite (Fe_3O_4) as the predominant iron oxide phase. Adsorption studies demonstrated equilibrium capacities of 24.63 mg g^{-1} for FeOHC and 18.70 mg g^{-1} for FeOHC-C, with adsorption kinetics best described by the Elovich model and equilibrium behavior fitting the Sips isotherm, suggesting a heterogeneous monolayer adsorption process. Thermodynamic analysis confirmed that adsorption was spontaneous and exothermic, primarily driven by physical interactions, including hydrogen bonding, π–π interactions, and electrostatic attraction. Fenton oxidation experiments revealed that 2-CP degradation was most efficient under acidic to neutral conditions (pH 3.0–6.0), diminishing drastically at alkaline conditions. The fact that good results were obtained at neutral pH demonstrates its practical applicability. Reusability tests confirmed the long-term stability of the materials, with FeOHC-C maintaining sustained catalytic performance over multiple cycles. These findings highlight the dual functionality of composites as efficient adsorbents and self-regenerating catalysts, offering a promising and scalable solution for the remediation of chlorinated organic pollutants in water.

Keywords Brewer's spent grain, Iron oxide, Carbon composite, Biomass, Hydrochar

The rapid advancement of industrial development has driven the creation of diverse products that, while offering significant benefits, have also introduced organic contaminants into aquatic environments[1]. Among these, chlorophenols (CPs) are classified as priority pollutants due to their high toxicity to plants, animals and humans even at low concentrations[2]. Key industries contributing to CP contamination include pulp and paper manufacturing, pharmaceuticals, agro-industries, and wastewater treatment facilities, where chlorination processes can generate these compounds as by-products[3]. Monochlorinated phenols, particularly 2-chlorophenol (2-CP), are among the most frequently detected pollutants in industrial wastewater[4]. Their chemical structure imparts high stability and resistance to natural degradation, allowing them to persist in the environment and exacerbate their ecological impact[5]. As a result, the efficient removal of 2-CP from water sources has become an environmental and public health challenge.

[1]Doctorate in Engineering Sciences with Specialization in Bioprocess, Chemical Engineering Department, Universidad de La Frontera, Francisco Salazar 01145, Temuco, Chile. [2]Chemical Engineering Department, Universidad de La Frontera, Francisco Salazar 01145, Temuco 4780000, Chile. [3]School of Engineering, Faculty of Sciences, Engineering and Technology, Universidad Mayor, Temuco, Chile. [4]Department of Chemical, Environmental and Materials Engineering, Biorefinery Research Institute (I3B), University of Jaén, Campus Las Lagunillas s/n, Jaén 23071, Spain. ✉email: mara.cea@ufrontera.cl

To address this issue, various water treatment technologies have been explored, including catalytic wet oxidation[6], ozonation and electrochemical degradation[7], biodegradation[8], and adsorption[9]. Among these, adsorption is widely recognized for its efficiency and versatility in removing a broad spectrum of contaminants[10]. However, traditional adsorption methods are non-destructive, merely transferring pollutants from one phase to another, leading to the accumulation of spent adsorbents that require costly regeneration or disposal as hazardous waste[11]. To overcome these limitations, integrating adsorption with oxidative treatments, such as heterogeneous Fenton reactions, has emerged as a promising approach[12]. This combined method not only regenerates the adsorbent material but also mitigates the challenges associated with homogeneous Fenton processes, which are constrained by narrow acidic pH ranges and produce substantial iron sludge[13]. Recent studies have shown that nano-sized iron oxide compounds supported on activated carbon further enhance the performance of these combined systems, improving degradation rates while minimizing secondary waste generation[14–17]. This synergistic approach offers a sustainable and effective strategy for treating wastewater contaminated with chlorophenols.

Traditionally, carbon materials have been synthesized using fossil-based precursors through methods such as chemical vapor deposition, arc discharge, and laser vaporization[18–20]. However, the growing need for sustainable and eco-friendly alternatives has shifted research focus on biomass-derived carbon materials, which are abundant, cost-effective, and environmentally friendly[21]. Among various biomass conversion techniques, hydrothermal carbonization (HTC) has gained attention due to its low energy requirements, minimal greenhouse gas emissions, and ability to produce highly porous and functionalized carbon materials[18,22]. Agricultural and industrial biowastes, such as brewer's spent grain (BSG) and brewery spent yeast (BSY), represent underutilized resources with significant potential for iron oxide/activated hydrochar composite production[23,24]. In Chile, the brewing industry generates substantial amounts of organic waste, presenting an opportunity to valorize these by-products into high-value materials for water treatment applications.

Thus, the objective of this study is to develop an efficient and sustainable method for removing 2-CP from wastewater by synthesizing iron oxide/activated hydrochar composites derived from BSG. This research evaluates the adsorption and heterogeneous Fenton degradation performance of these composites, addressing both water pollution mitigation and the valorization of industrial biowastes. By integrating renewable biomass sources with advanced material synthesis techniques, this study aims to contribute to the development of eco-friendly and high-performance solutions for wastewater treatment.

Materials and methods

Materials

Brewer's Spent Grain (BSG), obtained from a craft brewery in Freire, Chile, containing 80% of water was collected and stored at 4 °C to maintain its quality until use. The chemicals used in the study included iron nitrate ($Fe(NO_3)_3{\cdot}9H_2O$, ≥ 98%), iron sulfate ($FeSO_4{\cdot}7H_2O$, ≥ 99%), and hydrogen peroxide (H_2O_2, 30%wt.), all sourced from Sigma-Aldrich. High-purity (99.99%) nitrogen gas (N_2) was supplied by Indura company. The 2-CP used in the experiments was provided by Acros Organics, with a purity level > 99.9%.

Preparation of Iron oxide/activated hydrochar composites

The synthesis methodology for the iron oxide/activated hydrochar composite via the incipient wet impregnation (FeOHC), is outlined as follows. First, 200 ± 0.07 g of wet-BSG was suspended in 1,600 mL of deionized water, maintaining biomass-to-water ratio of 1:8. A mixture of iron salts ($Fe(NO_3)_3{\cdot}9H_2O$ and $FeSO_4{\cdot}7H_2O$) was added to the suspension in a 1:1 Fe^{3+}/Fe^{2+} molar ratio. The resulting mixture was transferred to a 3.8 L Parr 4581 reactor (Moline, IL, USA), equipped with a Parr 4848 PID temperature controller (Moline, IL, USA). The reactor was heated to 220 °C under continuous stirring at 100 rpm and maintained for 4 h. After the reaction, the heating was stopped, and the reactor was allowed to cool naturally. The resulting material was vacuum-filtered, washed with deionized water (3 × 50 mL), and dried at 105 ± 1 °C for 24 h. Additionally, pure hydrochar (HC) was synthesized following the same procedure, but without iron salt addition. For comparison, another composite (FeOHC-C) was synthesized using the co-precipitation method[25], where Fe_3O_4 nanoparticles were deposited onto the HTC-derived carbon support. This was achieved by mixing $Fe(NO_3)_3{\cdot}9H_2O$ and $FeSO_4{\cdot}7H_2O$ in an aqueous solution, followed by dropwise addition of NH_4OH to induce precipitation. The resulting composite was collected, washed, and dried.

Subsequently, all three materials (HC and FeOHC, FeOHC-C) were activated through pyrolysis at 400 °C for 2 h, using a N_2 flow rate of 1 L min^{-1}. In this process, 5 g of the materials were loaded into the reactor, and after the desired residence time, the reactor was cooled to room temperature. After pyrolysis, the materials were ground, sieved (particle size: 100–50 µm), and stored for further characterization and testing. A schematic representation of the synthesis process is provided in Fig. 1.

Material characterization

The synthetized materials were characterized using various techniques. Fourier Transform Infrared Spectroscopy (FTIR) was conducted using a Cary 630 FTIR (Agilent Technologies, USA). The superficial area and pore structure were analyzed by performing N_2 adsorption-desorption isotherms at 77 K using a Nova 1000e analyzer (Quantachrome Instruments, USA). The morphological characteristics of the materials were examined using scanning electron microscopy (SEM) SU-3500 (Hitachi, Japan) at an acceleration voltage of 10 kV, and their elemental composition was determined using energy dispersive X-ray spectroscopy (EDS). The chemical composition of the materials (CHNS) was determined using an elemental analyzer EA3000 (Eurovector, Italy), while the inorganic composition of the materials was analyzed by total reflection X-ray fluorescence (TXRF) in a Bruker S4 T-Star (Bruker, Germany) spectrometer. To determine the ash content thermogravimetric analysis (TGA) of materials was performed in a PerkinElmer STAR 6000 thermogravimetric balance under N_2

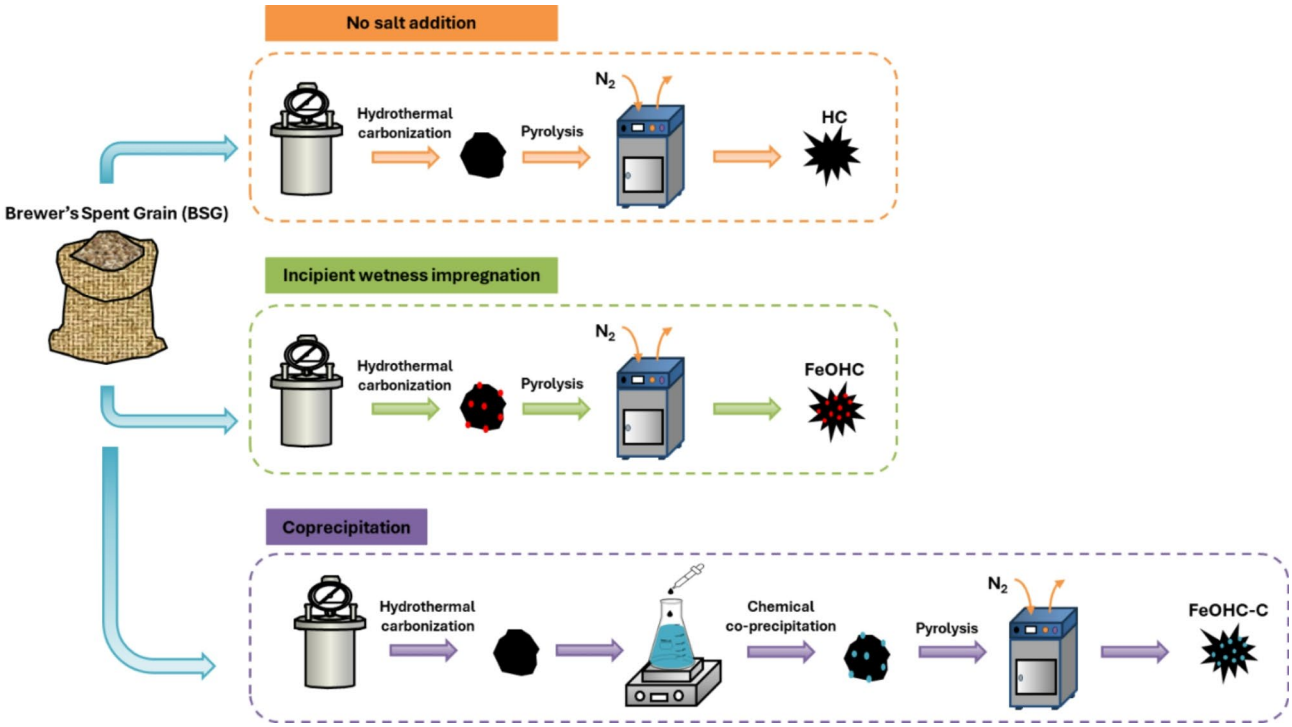

Fig. 1. Preparation process of the Iron Oxide/Activated Hydrochar composites.

atmosphere, and the isoelectric point (pH_{IEP}) was determined using a ZetaSizer Nano ZS (See Supplementary material S.1 for additional information).

Adsorption kinetics

The adsorption kinetics of 2-CP and the time required to reach equilibrium were evaluated through a series of experiments using the prepared materials. For each experiment, 25 mg of the adsorbent materials were added to 50-mL centrifuge tubes containing 25 mL of an aqueous solution of 2-CP (20 mg L^{-1}) adjusted to pH 6.0. The tubes were placed on a rotary shaker and agitated at 200 rpm under controlled conditions of 25 ± 1 °C.

At specific time intervals, aliquots were collected, filtered using 0.22 µm PVDF filters, and stored in vials at 4 °C for subsequent analysis. The residual concentrations of 2-CP were determined using high-performance liquid chromatography (HPLC) LC-4000 instrument (Jasco, Japan) equipped with an analytical C18 reversed-phase column, Inertsil ODS-4, 5 µm, 250 × 4.6 mm (Gl Science, Japan). The mobile phase consisted of a 1:1 (v/v) mixture of acetonitrile and 1% aqueous phosphoric acid solution, flowing at a rate of 1 mL min^{-1}. The column temperature was maintained at 35 °C, with the detector at 274 nm and an injection volume of 20 µL. Quantification of 2-CP was performed using a calibration curve.

Adsorption isotherms

Adsorption equilibrium experiments were conducted at 25 ± 1 °C to evaluate the capacity of the adsorbent materials. For each experiment, 25 mg of the adsorbent was mixed with 25 mL of 2-CP solutions, with initial concentrations varying between 10 and 100 mg L^{-1}, at pH 6.0. The mixtures were agitated at 200 rpm in a rotary shaker for 24 h to ensure equilibrium was reached. After equilibration, the supernatants were filtered through 0.22 µm PDVF filters and transferred to HPLC vials for analysis. The adsorption capacity (q_e), representing the amount of 2-CP adsorbed per gram of adsorbent, was calculated using the following equation:

$$q_e = \frac{(C_0 - C_e)\,V}{W} \tag{1}$$

Where q_e is the adsorption capacity at equilibrium (mg g^{-1}), C_0 and C_e are the initial and equilibrium concentrations of 2-CP, respectively (mg L^{-1}), V is the volume of solution (L), and W is the mass of adsorbent (g).

Evaluation of the heterogeneous Fenton reaction

The degradation efficiency of 2-CP via the heterogeneous Fenton catalytic reaction was evaluated. The procedure involved adding 25 mg of the iron oxide/activated hydrochar composite to 25 mL of a 2-CP solution (20 mg L^{-1}) and stirring the mixture at 200 rpm under controlled conditions at 25 °C. The reaction was initiated by introducing a specified amount of hydrogen peroxide (H_2O_2, 30 wt%) to achieve the desired final concentration.

At predetermined intervals, aliquots of the reaction mixture were filtered using 0.22 µm PVDF filters and stored in amber vials to prevent photodegradation for subsequent analysis. The effects of key reaction parameters, including H_2O_2 concentration (50–150 mM) and initial pH (3.0–9.0), on the degradation efficiency of 2-CP were systematically investigated to optimize the catalytic performance.

Reusability studies

The stability and reusability of the catalyst were evaluated over five consecutive Fenton reaction cycles at the best obtained conditions. At the end of each cycle, the catalyst was magnetically separated and washed with deionized water to remove any adsorbed residues. A fresh 2-CP solution at a concentration of 20 mg L^{-1} was then prepared, and a new dose of H_2O_2 was added to initiate the next reaction cycle. To assess the catalyst's activity loss over multiple cycles, 2-CP degradation was monitored using HPLC, and the removal efficiency was quantified in each cycle.

Results and discussion

Material characterization

Chemical properties of the materials

Table 1 presents the elemental composition of the synthesized materials: HC, FeOHC, and FeOHC-C. HC is characterized by its high carbon content (75.3 wt%), closely aligning with the synthesis reported by Olszewsky et al.[23]. using BSG under a similar methodology. As expected, the incorporation of iron led to a notable reduction in carbon content, decreasing to 34.1 wt% in FeOHC and 61.9 wt% in FeOHC-C. This iron addition also resulted in a significant increase in ash content, rising from 4.0 wt% in HC to 46.9 wt% in FeOHC and 18.4 wt% in FeOHC-C. Furthermore, both hydrogen and nitrogen contents slightly decreased in the iron-containing materials compared to HC, while oxygen content remained relatively consistent, ranging from 11.8 wt% to 13 wt% across all samples. A small sulfur content (0.29 wt%) was detected in FeOHC-C, attributed to the use of iron sulfate in the co-precipitation method. Iron content in the materials was determined to be 0.09 wt% for HC, 39.0 wt% for FeOHC, and 6.9 wt% for FeOHC-C, indicating that the hydrothermal impregnation method resulted in higher iron incorporation compared to the co-precipitation technique. Previous studies have demonstrated that the synthesis of carbon-metal composites via HTC facilitates the integration of iron into the hydrochar matrix due to the high temperature and pressure conditions of the process[26,27].

The isoelectric point (pH_{IEP}), determined via potentiometric titration, was 6.02 for HC, 6.30 for FeOHC, and 6.39 for FeOHC-C. The increase in pH_{IEP} observed in the iron-containing materials suggests surface properties closer to those of iron oxide minerals, such as magnetite (Fe_3O_4), which has an isoelectric point of 6.89[28].

FTIR and XRD analysis

FTIR analysis was performed to investigate the surface functional groups of all materials, with the results are illustrated in Fig. 2a.

The spectrum of BSG reveals a prominent band in the 3600–3300 cm^{-1} region, corresponding to O-H stretching vibrations from hydroxyl and carboxyl functional groups[29]. Additionally, intense vibrations in the 3000–2800 cm^{-1} region were observed, associated with aliphatic C-H functional group (CH_3- and CH_2-), which are characteristics of sp^3 vibrations within the lignin structure[29,30]. In contrast, the synthesized materials exhibit a marked reduction in transmittance intensity for these characteristic BSG bands, indicating oxidation reactions and dehydration processes in the lignocellulosic matrix[31]. This transformation results in the removal of O-H functional groups, increasing the hydrophobic character of the synthesized materials[23]. HC, FeOHC, and FeOHC-C display distinct absorption peaks at approximately 1578 cm^{-1}, 1027 cm^{-1}, and 624 cm^{-1}. The peak at ~ 1578 cm^{-1} corresponds to C = O stretching vibrations, consistently present across all materials[30]. The 1027 cm^{-1} peak, observed exclusively in FeOHC, is attributed to C-O stretching in carboxyl groups and C-OH bending vibration, suggesting the presence of oxygen-containing functional groups (e.g., hydroxyl, carboxyl,

Material	HC	FeOHC	FeOHC-C
Elemental analysis (wt%)			
C	75.3	34.1	61.9
H	4.21	3.05	3.39
N	4.63	2.94	3.78
O[a]	11.8	13.0	12.2
S	N.D.	N.D.	0.29
Proximate analysis (wt%)			
Ash	4.00	46.9	18.39
TXRF analysis (wt%)			
Fe	0.09	39.0	6.88
Isoelectric Point			
pH_{IEP}	6.02	6.30	6.39

Table 1. Chemical composition of HC, FeOHC, and FeOHC-C. [a]Obtained by difference: %O = 100 - (%C + %H + %N + %S + %Ash). N.D. Not detected.

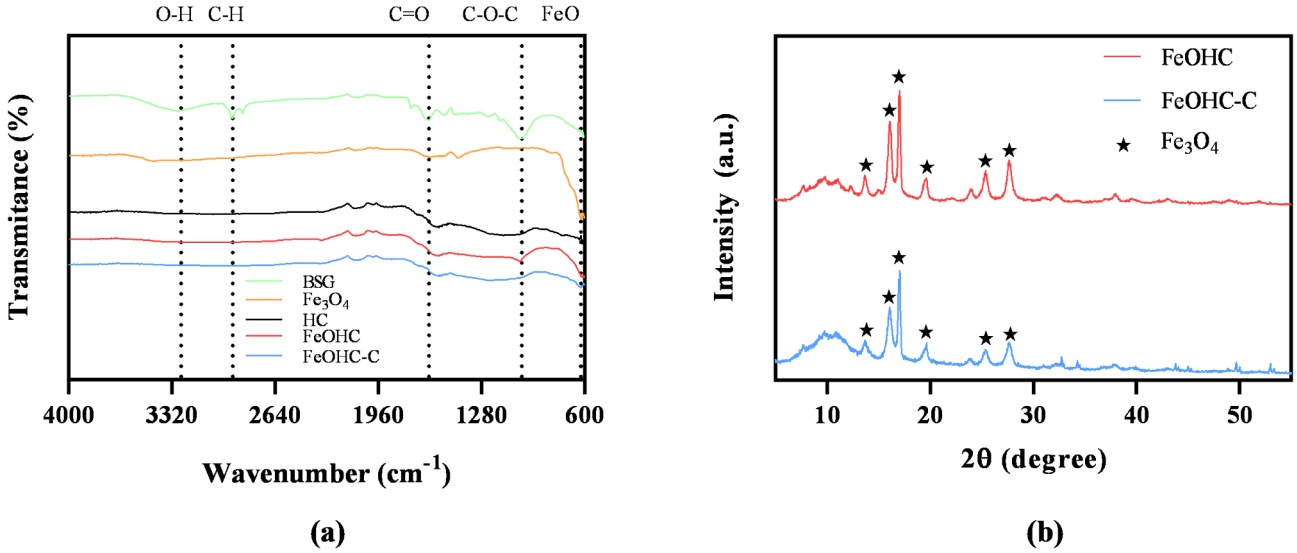

Fig. 2. (**a**) FTIR spectra of BSG, Fe_3O_4, HC, FeOHC, and FeOHC-C; (**b**) XRD patterns of the HC, FeOHC, and FeOHC-C.

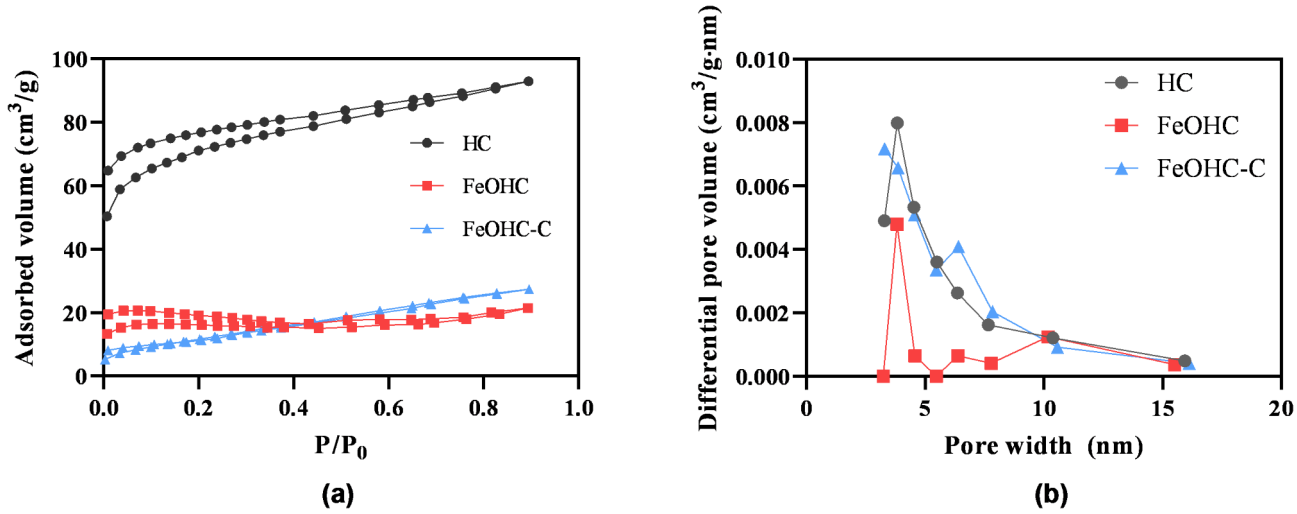

Fig. 3. (**a**) Adsorption/desorption isotherms of N_2 at 77 K; (**b**) Pore size distribution estimated with BJH method for HC, FeOHC, and FeOHC-C.

and carbonyl) that enhance the adsorption capacity for organic compounds[32,33]. Additionally, the peak at 624 cm^{-1}, characteristic of magnetite (Fe_3O_4) and iron oxide/activated hydrochar composites, correspond to Fe-O vibrations, confirming the successful incorporation of Fe_3O_4 onto the hydrochar surface[34,35]. It is worth noting that the broad peak around 2350 cm^{-1}, visible in all samples, results from atmospheric CO_2 interference.

The XRD patterns of the iron oxide/activated hydrochar composites are shown in Fig. 2b. Based on JCPDS Card No. 19–0629, the characteristic peaks at Bragg diffraction angles (2θ) of 13.7°, 16.1°, 17.0°, 19.7°, 25.4°, and 27.6° confirm the presence of Fe_3O_4 crystallites, corresponding to specific crystallographic planes (220), (311), (222), (400), (511), and (440)[36]. The XRD patterns further confirm the successful formation of magnetic Fe_3O_4 in both materials. No significant differences in the synthesized iron oxides were observed, indicating a uniform incorporation of Fe_3O_4 across the composites.

Surface and pore structure analysis

The key properties of materials to evaluate their suitability as adsorbents and catalysts include physical characteristics, specific surface area, and porosity. These parameters are typically determined using N_2 adsorption-desorption isotherms at 77 K, as depicted in Fig. 3a.

Based on the IUPAC classification, the synthetized materials exhibit a type IV(a) N_2 adsorption-desorption isotherms[37]. This type of isotherm is characteristic of predominantly mesoporous materials, with pores

diameters ranging from 2 to 50 nm and minimal microporosity (< 2 nm). It reflects the occurrence of multilayer adsorption and capillary condensation within the mesopores[38]. Such behavior is well-documented for activated hydrochar and iron oxide/activated hydrochar composites derived from biomass, which are widely recognized as mesoporous solids[39,40].

The pore size distribution (Fig. 3b) confirms the mesoporous nature of all synthesized materials. The pore sizes for HC, FeOHC, and FeOHC-C are centered around 4 nm[41]. Notably, FeOHC predominantly displays pores of approximately 4 and 10 nm, indicating a high degree of uniformity. In contrast, HC and FeOHC-C exhibit less uniform pore distributions, with pore sizes ranging between 3 and 15 nm. The specific surface area (S_{BET}), total pore volume (V_p), and average pore diameter (D_p) of the synthesized materials are summarized in Table 2. BET analysis revealed a reduction in the S_{BET} of HC from 259.16 $m^2\ g^{-1}$ to 66.7 $m^2\ g^{-1}$ for FeOHC and 44.9 $m^2\ g^{-1}$ for FeOHC-C. This decrease is attributed to pore blockage caused by the incorporation of iron oxide particles, with the effect being more pronounced in FeOHC-C due to the precipitation of iron oxides on the surface[42]. The D_p for HC, FeOHC, and FeOHC-C were 3.83, 3.82, and 3.29 nm, respectively, while the V_p range from 0.029 to 0.012 $cm^3\ g^{-1}$. The addition of iron salts during HTC likely contributed to the formation of iron oxides within the hydrochar pores, reducing the available void space[43] Additionally, the chemical co-precipitation method may have influenced the pore structure due to particle agglomeration on the hydrochar surface[44]. These findings suggest that the synthesized composites are promising candidates for adsorbing 2-CP. The molecular diameter of 2-CP is approximately 5.7 Å, significantly smaller than the average pore diameters of the materials, which are seven times larger. This size disparity facilitates the diffusion of 2-CP molecules into the pores, enabling effective adsorption on the material's surface.

SEM-EDS analysis

SEM analysis was conducted to examine the morphology of the synthesized samples, as shown in Fig. 4. The micrographs reveal the iron oxide/activated hydrochar composites with a heterogeneous distribution of pores varying in size, shape, and dimensions across the surface. Both FeOHC and FeOHC-C samples exhibit irregular surface structures, likely due to the release of volatiles and the formation of cavities during the HTC and pyrolysis processes. Notably, the FeOHC composite displayed nanometer-scale agglomerations of Fe_3O_4 particles on the surface of the carbonaceous matrix (Fig. 4a), suggesting that the integration of Fe_3O_4 into the structure was effectively promoted during the HTC process. In contrast, the FeOHC-C composite showed smaller Fe_3O_4 agglomerations due to the specific synthesis methodology employed (Fig. 4b). Additionally, larger pores were observed in FeOHC, indicating less cavity blockage compared to FeOHC-C[45]. To further analyze the distribution of iron on the surface of the composites, EDX mapping was performed (Fig. 4c and d). The results revealed a heterogeneous distribution of iron across the surfaces of both materials.

Evaluation of adsorptive properties of synthesized materials

Adsorption kinetic studies

Adsorption kinetics are essential for understanding the temporal dynamics of contaminant removal from water. In this study, the adsorption behavior of 2-CP onto the synthesized materials was investigated over 24 h, as shown in Fig. 5. The adsorption process exhibited two distinct phases: an initial rapid phase characterized by the swift removal of 2-CP due to the high availability of accessible adsorption sites on the material surfaces, followed by a slower phase where the removal rate decreased as these active sites became progressively saturated. Equilibrium was achieved at approximately 3 h for FeOHC, whereas HC and FeOHC-C required nearly 10 h to stabilize[46].

The adsorption capacities of the materials followed the trend HC > FeOHC > FeOHC-C, with maximum capacities of 15.4, 7.71, and 5.14 mg g^{-1}, respectively. These results align with literature data, highlighting the importance of surface area and surface reactivity in adsorption processes[47]. HC's superior adsorption performance can be attributed to its more active surface compared to the FeOHC and FeOHC-C composites. While the iron oxide/activated hydrochar composites demonstrated lower adsorption capacities, the incorporation of magnetite provides catalytic properties that enhance their functional versatility, particularly for applications involving the catalytic degradation or transformation of pollutants.

To evaluate the adsorption kinetics of 2-CP on the synthesized materials, the experimental data were fitted to four widely used kinetic models: pseudo-first-order (PFO), pseudo-second-order (PSO), Elovich, and intraparticle diffusion models, represented by Eqs. 2–5:

$$q_t = q_1 \cdot \left(1 - e^{-k_1 \cdot t}\right) \tag{2}$$

Materials	S_{BET} [a] ($m^2\ g^{-1}$)	V_p [b] ($cm^3\ g^{-1}$)	D_p [b] (nm)
HC	259.2	0.028	3.83
FeOHC	66.61	0.012	3.82
FeOHC-C	44.96	0.029	3.29

Table 2. Textural properties of the materials. [a]Specific surface area (S_{BET}) was determined with nitrogen by multi-point BET method. [b]Total pore volume (V_p) and average pore diameter (D_p) was determined by BJH method.

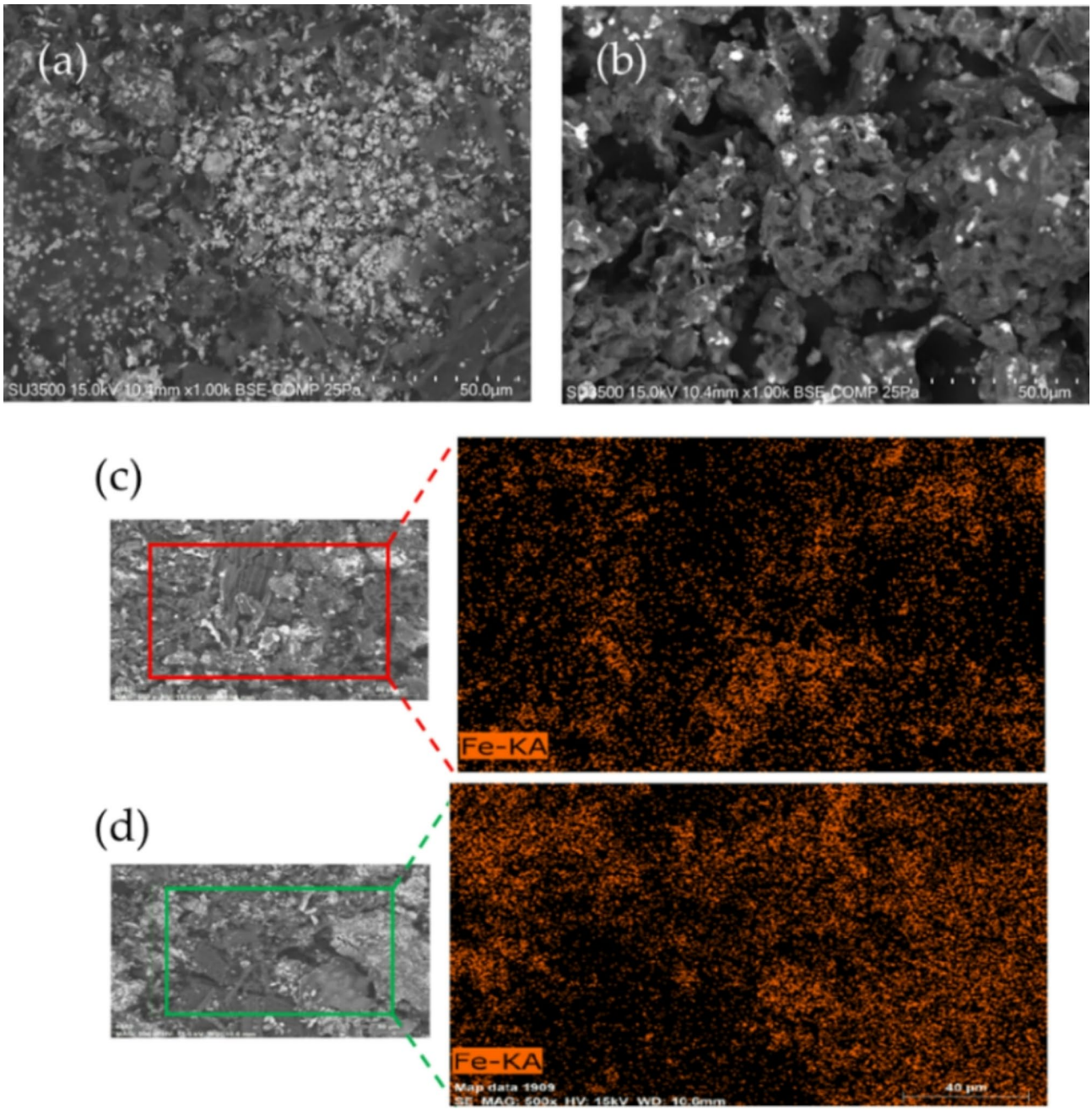

Fig. 4. SEM micrographs of (**a**) FeOHC, (**b**) FeOHC-C, and EDX-mapping micrographs of (**c**) FeOHC, (**d**) FeOHC-C.

$$q_t = \frac{q_2^2 \cdot k_2 \cdot t}{1 + q_2 \cdot k_2 \cdot t} \tag{3}$$

$$q_t = \frac{1}{\beta} \cdot ln\left(1 + \alpha \cdot \beta \cdot t\right) \tag{4}$$

$$q_t = k_3 \cdot t^{0.5} + C \tag{5}$$

Here, q_t (mg g^{-1}) is the adsorbed amount of 2-CP at time t; q_1 and q_2 (mg g^{-1}) are the equilibrium adsorption capacities for PFO and PSO models, respectively; k_1 (h^{-1}) and k_2 (g mg^{-1} h^{-1}) are the rate constants for PFO and PSO models, respectively; α (mg g^{-1} min^{-1}) and β (g mg^{-1}) are the initial adsorption rate constant and surface coverage-related parameter in the Elovich model; k_3 (mg g^{-1} $min^{-0.5}$) and C (mg g^{-1}) are the intraparticle diffusion constant and boundary layer thickness parameter, respectively.

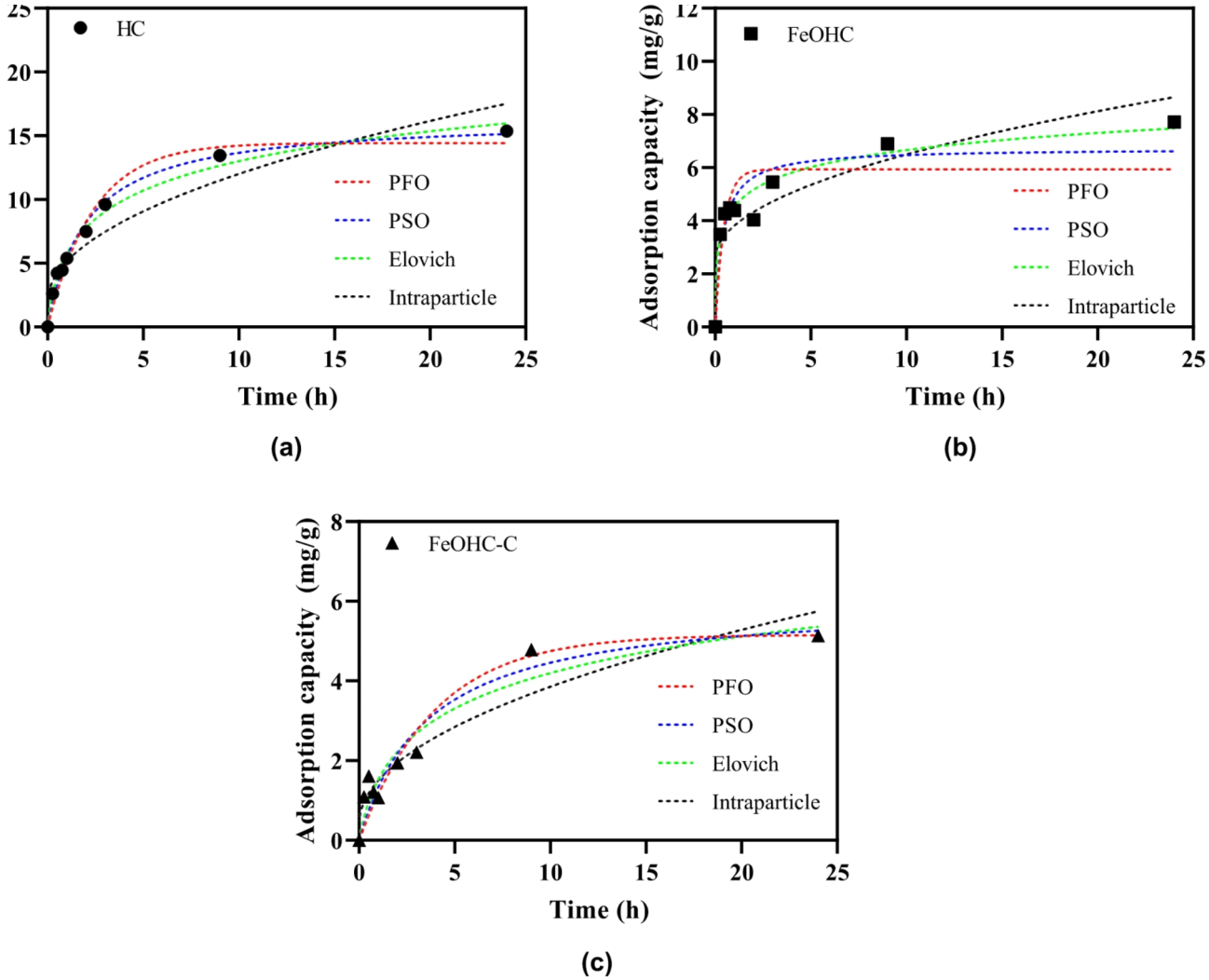

Fig. 5. Adsorption kinetic curves of 2-chlorophenol adsorption on (**a**) HC, (**b**) FeOHC, and (**c**) FeOHC-C materials (T = 298 K, pH = 6.0, adsorbent mass = 25 mg, [2-CP] = 20 mg L^{-1}, rpm = 200).

Non-linear regression analysis was conducted using MATLAB R2022b, with the resulting kinetic parameters summarized in Table 3. Among the models, the Elovich equation provide the best fit for all materials, evidenced by the highest correlation coefficients (R^2: 0.925–0.991) and the lowest Root Mean Square Error (RMSE: 0.496–0.517). The Elovich parameters revealed critical insights into adsorption dynamics where the initial adsorption rate (α) was highest for FeOHC, indicating a fast initial adsorption of 2-CP. Additionally, its higher number of sites available (β) suggests that this material has more available adsorption sites compared to HC and FeOHC-C[46]. The α/β ratio from the Elovich model provides key insights into the adsorption kinetic mechanism of the studied materials. FeOHC exhibits the highest ratio (≈ 111.5), indicating a rapid initial adsorption rate but a faster saturation of active sites, consistent with its equilibrium adsorption capacity. In contrast, HC presents a moderate ratio (≈ 50.8), suggesting a balanced adsorption rate with a more gradual site occupancy. FeOHC-C, with the lowest ratio (≈ 3.82), demonstrates a slower initial adsorption rate, likely due to diffusion limitations or reduced accessibility to active sites. Furthermore, the experimental pH (6.0) was slightly below the isoelectric point of the materials, resulting in a positively charged surface. This condition favored the electrostatic attraction of the negatively charged 2-CP species, enhancing adsorption efficiency.

Adsorption isotherms

An adsorption isotherm describes the relationship between the amount of adsorbate retained on the surface of the adsorbent and its equilibrium concentration in the liquid phase. Figure 6 presents the equilibrium adsorption isotherms for 2-CP on the synthesized materials. The experimental data obtained at 298 K were fitted to four isotherm models: Langmuir (Eq. 6), Freundlich (Eq. 7), Sips (Eq. 8), and Redlich-Peterson (Eq. 9).

$$q_e = \frac{q_m \cdot K_L \cdot C_e}{1 + K_L \cdot C_e} \tag{6}$$

Model	Parameter	HC	FeOHC	FeOHC-C
PFO	q_1 (mg g^{-1})	14.43	5.949	5.157
	k_1 (h^{-1})	0.422	2.194	0.253
	R^2	0.969	0.709	0.915
	RMSE	0.952	1.170	0.537
PSO	q_2 (mg g^{-1})	16.40	6.725	6.041
	k_2 (g mg^{-1} h^{-1})	0.030	0.381	0.046
	R^2	0.989	0.860	0.921
	RMSE	0.547	0.876	0.521
Elovich	α (mg g^{-1} h^{-1})	14.78	120.0	2.779
	β (g mg^{-1})	0.291	1.076	0.728
	R^2	0.991	0.955	0.925
	RMSE	0.517	0.496	0.504
Intraparticle diffusion	k_3 (mg g^{-1} $h^{-0.5}$)	3.172	1.241	1.090
	C	1.974	2.575	0.406
	R^2	0.906	0.733	0.909
	RMSE	1.650	1.210	0.556

Table 3. Kinetic parameters for 2-CP adsorption onto different adsorbents.

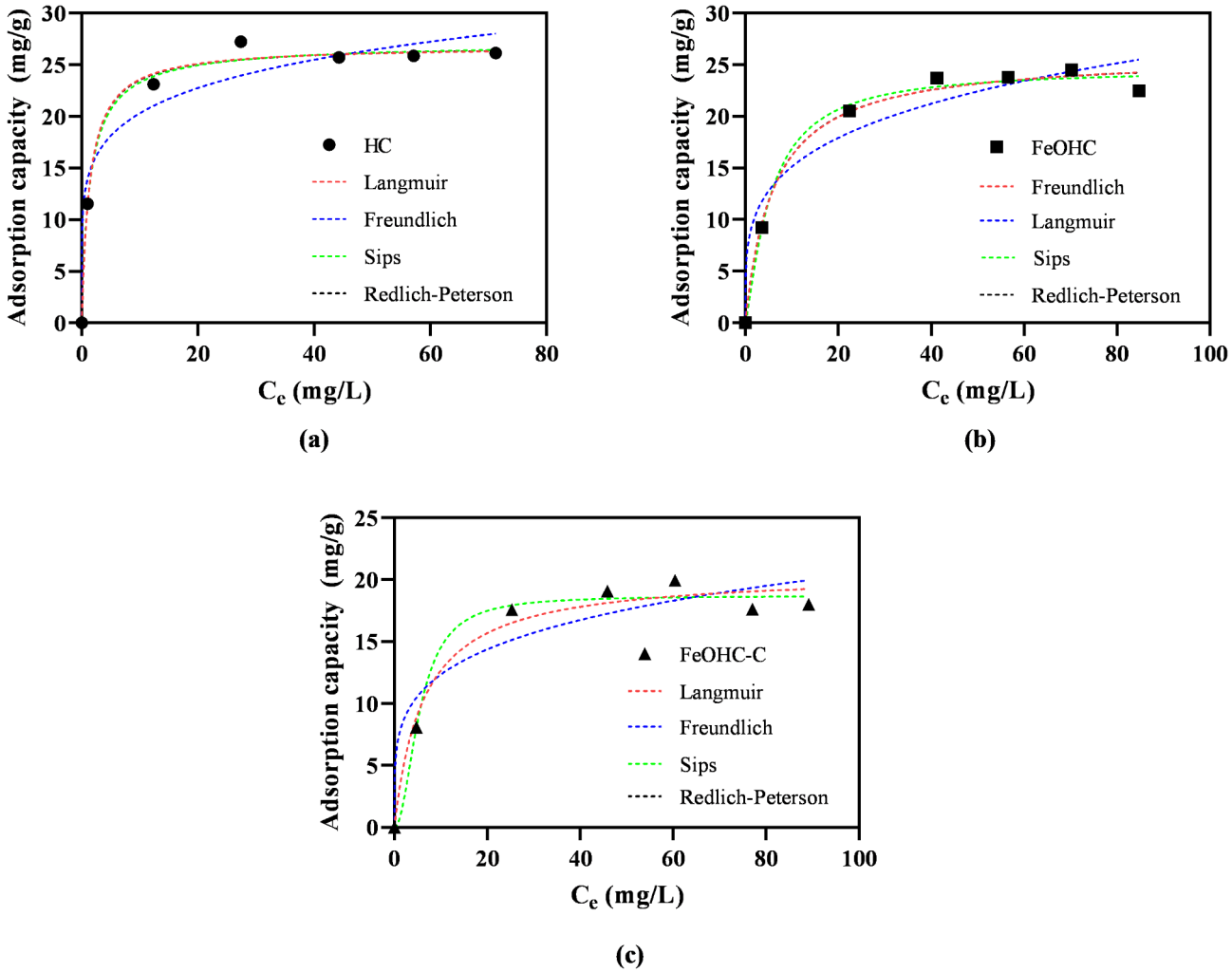

Fig. 6. Adsorption isotherms of 2-chlorophenol on (**a**) HC, (**b**) FeOHC, and (**c**) FeOHC-C materials (T = 298 K, pH = 6.0, adsorbent mass = 25 mg, rpm = 200).

$$q_e = K_f \cdot C_e^{1/n_F} \tag{7}$$

$$q_e = \frac{q_{sat} \cdot b \cdot C_e^{1/n}}{1 + b \cdot C_e^{1/n}} \tag{8}$$

$$q_e = \frac{K_R \cdot C_e}{1 + \alpha_R \cdot C_e^{\beta}} \tag{9}$$

Where q_e is the adsorbed quantity per unit mass of adsorbent (mg g^{-1}), and C_e (mg L^{-1}) is the equilibrium adsorbate concentration; In the Langmuir model, q_m (mg g^{-1}) is the maximum monolayer adsorption capacity, and K_L (L mg^{-1}) is the Langmuir constant; The Freundlich model uses, K_F (L mg^{-1}) as isotherm constant and n_F as the adsorption intensity; The Sips model includes q_{sat} (mg g^{-1}) for saturation adsorption capacity, *1/n* as a model exponent, and *b* (L mg^{-1}) as a constant; In the Redlich-Peterson model, K_R and α_R (L mg^{-1}) are constants and *b* is a nondimensional exponent with a value ranging from 0 to 1.

The adsorption isotherm parameters were determined through non-linear regression analysis using MATLAB R2022b (Table 4). Among the evaluated models, the Sips isotherm exhibited the best fit across all synthesized materials, demonstrating high correlation coefficients (R^2 = 0.989–0.994) and low root mean square errors (RMSE = 0.978–1.007). This strong agreement suggests that the adsorption process follows a hybrid mechanism incorporating both Langmuir-like monolayer coverage and Freundlich-type surface heterogeneity. Further analysis of the Sips model confirmed the formation of a 2-CP monolayer on the adsorbent surfaces, with maximum adsorption capacities (q_{sat}) values of 27.16 mg g^{-1} for HC, 24.63 mg g^{-1} for FeOHC, and 18.70 mg g^{-1} for FeOHC-C. The observed reduction in adsorption capacity upon Fe_3O_4 incorporation indicates that iron oxide particles partially obstruct active adsorption sites, consistent with the lower specific surface areas measured via BET analysis.

The heterogeneity parameter (*n*) in the Sips model provides insights into the surface uniformity of the adsorbents. When $n \approx 1$, the Sips model converges to the Langmuir isotherm, implying a relatively homogeneous surface. In contrast, $n < 1$ signifies increasing heterogeneity due to the presence of adsorption sites with varying affinities[48]. The HC material exhibited near-homogeneity characteristics ($n = 1.091$, $R^2 = 0.993$), closely aligning with the Langmuir model ($R^2 = 0.994$). However, FeOHC and FeOHC-C displayed significantly greater surface heterogeneity, with $n = 0.791$ and $n = 0.487$, respectively. These findings suggest that HTC produces a highly uniform adsorbent surface, whereas the incorporation of Fe_3O_4, particularly through chemical co-precipitation, introduces structural irregularities that enhance heterogeneity. The results underscore the critical influence of synthesis methods on the physicochemical properties of adsorbents and their subsequent adsorption performance.

Table 5 summarizes the maximum adsorption capacity (q_{max}) of 2-CP on various materials. In our study, HC and FeOHC exhibited q_{max} of 27.16 mg g^{-1} and 24.63 mg g^{-1}, respectively, positioning them competitively among previously reported adsorbents. These values surpass those reported for coconut pith carbon (< 17.58 mg g^{-1})[49] and banana-derived activated carbon (24.33 mg g^{-1})[50], and are comparable to *Adenopus breviflorus* seeds (25.94 mg g^{-1})[4]. Nonetheless, their adsorption capacity is notably lower than *Croton caudatus*-derived activated carbon (53.62 mg g^{-1})[51], and significantly lower than magnetic composite carbon xerogels (130 mg g^{-1})[52]. This comparison highlights the potential of HC and FeOHC as effective adsorbents for 2-CP removal, demonstrating

Model	Parameter	HC	FeOHC	FeOHC-C
Langmuir	q_m (mg g^{-1})	26.81	25.99	20.60
	K_L (L mg^{-1})	0.733	0.164	0.160
	R^2	0.994	0.991	0.976
	RMSE	0.913	0.991	1.262
Freundlich	K_F (L mg^{-1})	13.92	8.611	7.434
	n_F	6.100	4.089	4.544
	R^2	0.959	0.951	0.926
	RMSE	2.271	2.278	2.215
Sips	q_{sat} (mg g^{-1})	27.16	24.63	18.70
	n	1.091	0.791	0.487
	b (L mg^{-1})	0.726	0.118	0.031
	R^2	0.993	0.993	0.989
	RMSE	1.007	0.986	0.978
RP	K_R (L mg^{-1})	19.87	4.299	3.287
	α_R (L mg^{-1})	0.749	0.166	0.159
	β	0.997	1.000	1.000
	R^2	0.994	0.991	0.976
	RMSE	1.021	1.111	1.411

Table 4. Fitting parameters for the adsorption isotherm data of 2-CP adsorption onto different adsorbents.

Material	q_{max} (mg g^{-1})	Reference
Coconut pith carbon	< 17.58	[49]
Banana-derived activated carbon	24.33	[50]
Adenopus breviflorus	25.94	[4]
Croton caudatus-derived activated carbon	53.62	[51]
Magnetic composite carbon xerogels	130.0	[52]
HC	27.16	This work
FeOHC	24.63	This work

Table 5. Comparison of the maximum adsorption capacity of 2-CP by HC, and FeOHC, with other reported results.

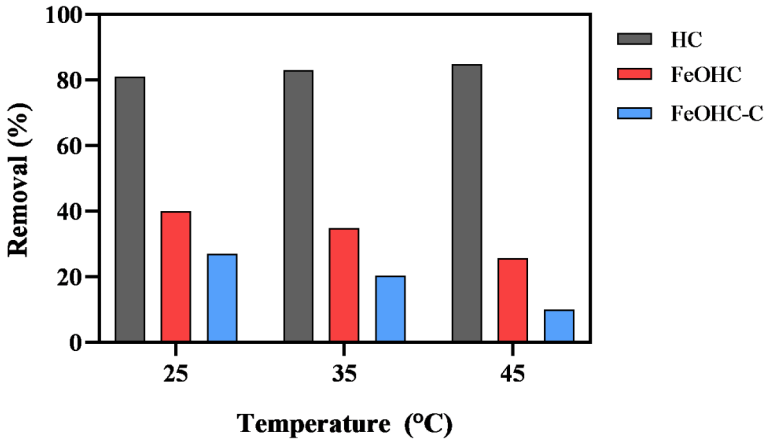

Fig. 7. Effect of temperature on 2-chlorophenol adsorption onto HC, FeOHC, and FeOHC-C materials (pH = 6.0, adsorbent mass = 25 mg, [2-CP] = 20 mg L^{-1}, rpm = 200).

competitive adsorption capacity within the mid-range of reported materials. While their performance is not as high as certain specialized adsorbents, their simple synthesis and tunable properties may offer practical advantages in industrial wastewater treatment.

Thermodynamic parameters for 2-CP adsorption

The calculation of thermodynamic parameters provides crucial insights into the sorption mechanisms. Numerous studies have assessed adsorption at different temperatures to identify the mechanisms controlling the sorption across different surfaces. In this study, adsorption experiments were conducted at 25, 35, and 45 °C to investigate the temperature dependence of 2-CP adsorption on the synthesized materials (Fig. 7).

The adsorption capacity of HC remains constant across the tested temperature range, indicating a temperature-independent adsorption mechanism. In contrast, adsorption capacity declined with increasing temperature for the iron oxide/activated hydrochar composites, dropping from 40 to 26% for FeOHC and from 27 to 9.9% for FeOHC-C. This decreasing trend suggests that 2-CP adsorption on iron oxide-containing materials is spontaneous and exothermic. Conversely, the behavior observed in HC implies that an energy input is required to initiate adsorption, indicating an endothermic process[46]. The diminished adsorption efficiency of the iron-containing materials at elevated temperatures may be attributed to the weakening of adsorption forces between the active sites of the adsorbent and the 2-CP molecules, reducing their retention[51]. This phenomenon aligns with previous findings, where a decrease in the adsorption of phenolic compounds has been observed in magnetic-activated carbons derived from pomegranate and corn husks[53,54].

To further confirm these observations, the standard Gibbs free energy change (ΔG°), entropy (ΔS°) and enthalpy (ΔH°) were determined using the following equations:

$$\Delta G^{\circ} = -RT \cdot lnK_c \tag{10}$$

$$lnK_c = \frac{\Delta S^{\circ}}{R} - \frac{\Delta H^{\circ}}{RT} \tag{11}$$

Where K_c is the equilibrium constant that can be calculated ad q_e/c_e for each temperature, T is the absolute temperature (K), and R is the universal gas constant (8.314 J mol^{-1} k^{-1}). ΔH° and ΔS° are calculated from the slope and intercept of the plots of ln(K_c) vs. 1/T, respectively.

As presented in Table 6, all Gibbs free energy values (ΔG°) were negative, confirming that the adsorption of 2-CP onto all synthesized materials is thermodynamically favorable and spontaneous[51]. The negative ΔH°

Materials	ΔH° (kJ mol^{-1})	ΔS° (kJ mol-1 K^{-1})	ΔG° (kJ mol^{-1})		
			293 K	308 K	318 K
HC	11.20	0.107	-20.67	-21.75	-22.80
FeOHC	-75.89	-0.158	-18.54	-16.08	-15.43
FeOHC-C	-65.29	-0.200	-16.40	-14.18	-12.41

Table 6. Thermodynamics parameters for 2-CP adsorption on C, FeOHC and FeOHC-C.

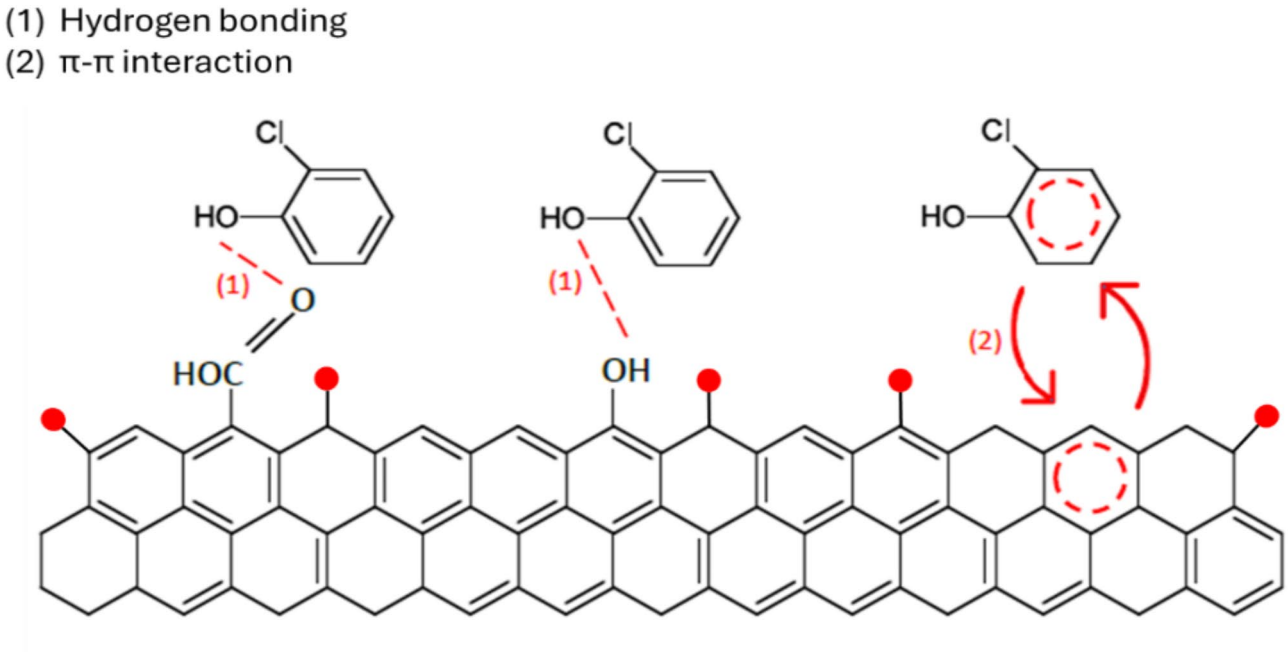

Fig. 8. Schematic of the possible interaction between 2-CP molecules and the surface of iron oxide/activated hydrochar composites.

values for FeOHC and FeOHC-C indicate an exothermic process consistent with the observed decreased in adsorption capacity at higher temperatures. In contrast, HC exhibited positive ΔH° values, supporting the notion that its adsorption process is endothermic. Furthermore, the absolute values of ΔH°, ranging from 11.20 to 75.89 kJ mol^{-1}, suggest that the adsorption occurs primarily thought physical adsorption. Typically, chemisorption processes require significantly higher enthalpy values, ranging from 80 to 450 kJ mol^{-1}[55]. These findings underscore the crucial role of material composition and surface chemistry in determining adsorption mechanisms and thermodynamic behavior.

Adsorption mechanisms of 2-CP on HC and Iron oxide/activated hydrochar composites

The adsorption of 2-CP onto HC and iron oxide/activated hydrochar composites involves multiple mechanisms, including hydrogen bonding between the phenolic hydroxyl group of 2-CP and oxygenated functional groups (carboxyl and hydroxyl) on the adsorbents, π–π interactions between the benzene ring of 2-CP and the graphitic domains of the carbon surface, and electrostatic attraction between the charged functional groups of the adsorbent and the phenolic groups of 2-CP (Fig. 8)[51]. FTIR spectroscopy confirms the presence of oxygenated functional groups, including carboxyl, hydroxyl, and aromatic rings, which actively participate in these interactions. The contribution of these functional groups suggests that surface chemistry plays a crucial role in adsorption performance. Additionally, the incorporation of iron oxide may introduce further adsorption pathways, such as surface complexation or Lewis acid-base interactions, potentially enhancing affinity toward 2-CP molecules[56]. Moreover, electrostatic interactions also play a crucial role, as indicated by the isoelectric point (pH_{IEP}) values of the synthesized materials—6.02 for HC, 6.30 for FeOHC, and 6.39 for FeOHC-C—and the pKa of 2-CP (8.52). At acidic pH, 2-CP remains predominantly neutral, favoring adsorption, whereas at alkaline pH, it becomes anionic, leading to a decrease in adsorption capacity due to electrostatic repulsion as the adsorbent surface becomes negatively charged. When pH exceeds the pH_{IEP}, this repulsion intensifies, further reducing adsorption efficiency[30]. These combined interactions—hydrogen bonding, π–π interactions, and electrostatic forces—synergistically enhance the affinity between the adsorbent materials and 2-CP, providing valuable insights into optimizing adsorption conditions for effective pollutant removal.

Catalyst test of Iron oxide/activated hydrochar for heterogeneous Fenton reaction

Effects of operational parameters

The degradation of 2-CP via heterogeneous Fenton oxidation reactions was evaluated under varying reaction time, H_2O_2 concentration, and pH (Fig. 9). As shown in Fig. 9a, the reaction follows a characteristic two-stage pattern: an initial rapid degradation phase, followed by a slower phase that eventually stabilizes, suggesting a progressive depletion of active catalytic sites or reaction efficiency over time. Notably, within the first hour, the synthesized materials achieved approximately 40% removal of 2-CP, with no significant difference between synthesis methods. Compared to adsorption alone, which required over 24 h to reach the same 40% removal, the Fenton oxidation process significantly reduces operational time, highlighting its efficiency.

Figure 9b illustrates the impact of pH on 2-CP degradation using FeOHC and FeOHC-C, confirming that catalytic activity in heterogeneous Fenton systems is strongly pH-dependent, as reported in previous studies[57]. The highest removal efficiencies were observed at pH 3.0, where FeOHC and FeOHC-C achieved 35% and 29% removal, respectively, after one hour at 25 °C. However, as the pH increased, degradation efficiency declined markedly, reaching a minimum at pH 9.0 (13% for FeOHC and 9% for FeOHC-C). This trend aligns with the well-established behavior of Fenton reactions, where acidic conditions favor hydroxyl radical generation, while higher pH values promote iron precipitation, reducing catalytic activity and overall pollutant degradation efficiency. However, the ANOVA analysis indicated no statistically significant differences in 2-CP removal between pH 3.0 and pH 6.0 for both synthesized materials, reinforcing the effectiveness of carbonaceous composites in the degradation of organic pollutants through heterogeneous Fenton reactions. This finding highlights their potential applicability in advanced water treatment processes.

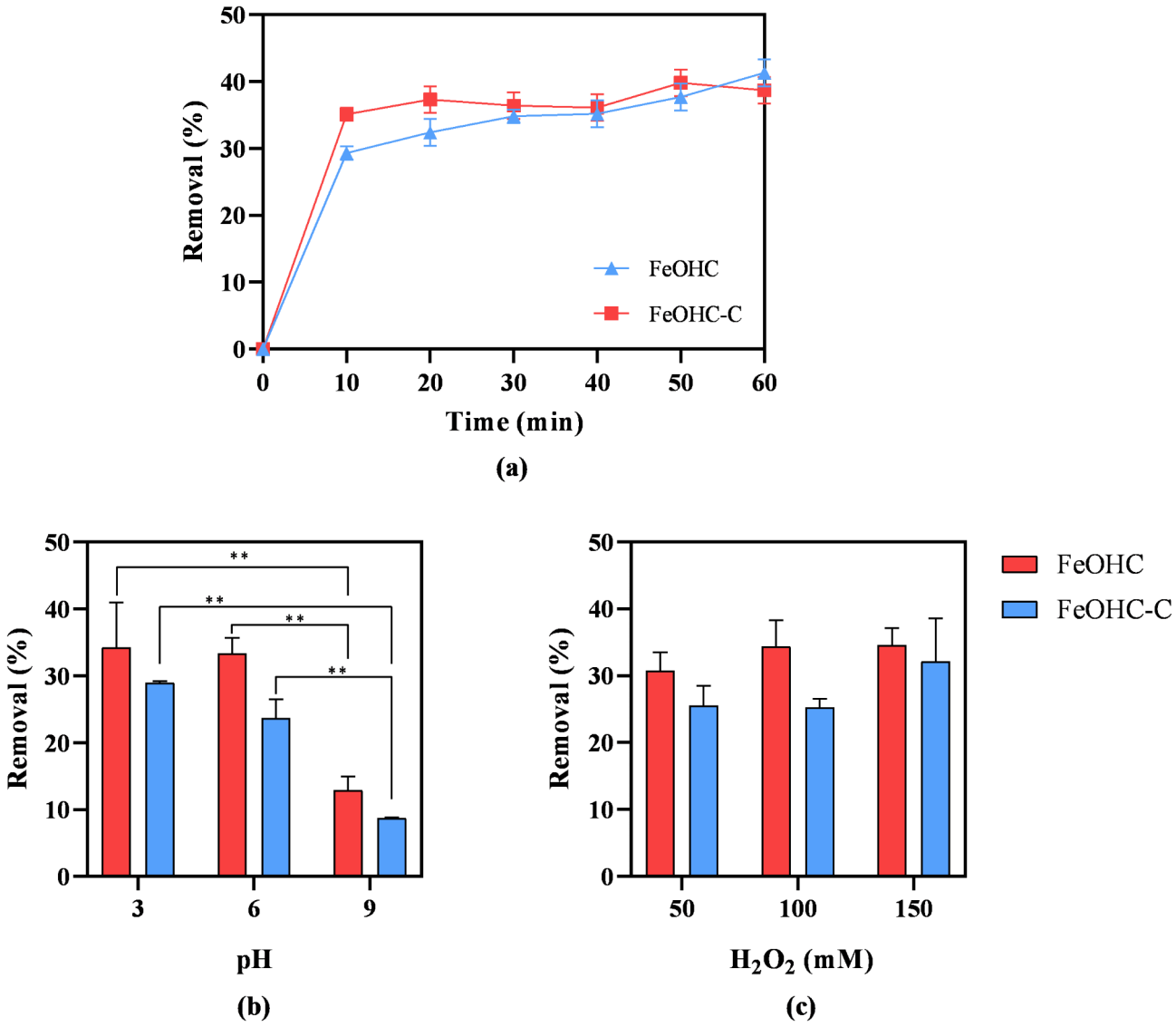

Fig. 9. Effect of (**a**) time, (**b**) pH and (**c**) H_2O_2 concentration on heterogeneous Fenton reaction (catalyst mass = 25 mg, [2-CP] = 20 mg L^{-1}, rpm = 200, Tukey's multiple comparison test: **: $p < 0.01$).

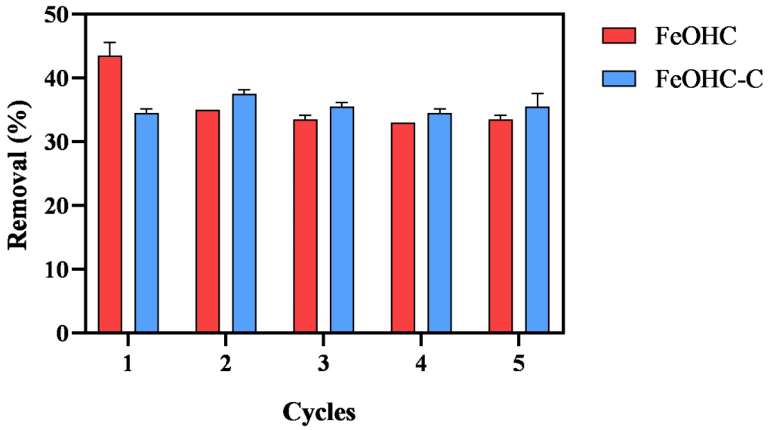

Fig. 10. Reutilization studies of 2-CP oxidation via heterogeneous Fenton reactions with iron oxide/activated hydrochar composites (catalyst mass = 25 mg, $[H_2O_2] = 150$ mM, pH = 6.0, [2-CP] = 20 mg L^{-1}, rpm = 200).

In Fenton systems, hydroxyl radicals (•OH) play a crucial role in organic contaminant degradation. The leaching of Fe^{2+}/Fe^{3+} ions from the hydrochar surface significantly contributed to the generation of these radicals. At pH 3.0, enhanced Fe^{2+} dissolution facilitated the formation of •OH radicals leading to greater 2-CP removal efficiency[58]. This process follows the reaction:

$$Fe^{2+} + H_2O_2 \rightarrow Fe^{3+} + OH^- + \bullet OH \quad (12)$$

Under acidic conditions, Fe^{2+} is readily released from Fe_3O_4, while the formation of ferric hydroxides ($Fe(OH)_3$) is inhibited, sustaining high catalytic activity. However, at pH levels above 6.0, the oxidation potential of •OH radicals decrease, and H_2O_2 undergoes rapid decomposition into O_2 and H^+, reducing its efficiency as an oxidant and consequently diminishing pollutant removal[58].

The effect of H_2O_2 concentration on 2-CP degradation was evaluated within the range of 50–150 mM (Fig. 9c). The results demonstrated a positive correlation between increasing H_2O_2 concentration and pollutant removal, with iron oxide/hydrochar composites exhibiting a linear trend in degradation efficiency. At lower H_2O_2 levels, the insufficient generation of •OH radicals resulted in limited removal performance. Conversely, at 150 mM H_2O_2, the higher radical production significantly enhanced 2-CP degradation, achieving maximum removal efficiencis of 37% and 27% for FeOHC and FeOHC, respectively. Despite this trend, no statistically significant differences were observed between removal efficiencies at varying H_2O_2 concentration, suggesting that beyond a certain threshold, excess of H_2O_2 may act as scavenger, consuming •OH radicals and limiting further degradation.

Based on these findings, a possible reaction mechanism for 2-CP degradation via iron oxide/hydrochar composites is proposed:

$$\equiv Fe^n - \text{oxide} + H_2O_2 \rightarrow \equiv Fe^{n+1} - \text{oxide} + OH^- + \bullet OH \quad (13)$$

$$\equiv Fe^{n+1} - \text{oxide} + H_2O_2 \rightarrow \equiv Fe^n - \text{oxide} + HO_2\bullet + H+ \quad (14)$$

Hydroxyl radicals are generated through the reaction of H_2O_2 with Fe(II) sites on the catalyst surface, as well as Fe^{2+} ions dissolved in the bulk solution. The reduction of Fe(III) back to Fe(II) ensures the continuous regeneration of active catalytic sites, maintaining the reaction cycle. Therefore, the heterogeneous Fenton system facilitates contaminant removal through two complementary mechanisms: (1) adsorption of 2-CP onto the composite surface and (2) catalytic oxidation via •OH radicals, leading to pollutant mineralization and desorption of degradation byproducts. This dual-action mechanism underscores the efficiency of iron oxide/hydrochar composites as sustainable catalysts for water purification applications.

Reusability of Iron-Oxide/Hydrochar composites via heterogeneous Fenton reaction

A key factor in the practical application of catalysts is their reusability. Therefore, the reusability of iron oxide/hydrochar composites for 2-CP removal was assessed under the optimal conditions determined in previous experiments (pH 6.0, H_2O_2 50 mM). As depicted in Fig. 10, FeOHC exhibited a decline in removal efficiency from 43 to 33% after two reuse cycles. This significant decrease in performance during the second cycle can be attributed to the detachment of weakly bound iron species from the composite surface during the initial reaction, reducing the availability of catalytic active sites. However, the residual iron remained catalytically active in subsequent cycles, maintaining some level of degradation efficiency. In contrast, FeOHC-C demonstrated superior stability, sustaining a removal efficiency between 35% and 37% across five consecutive cycles. This suggests that the iron species were more robustly anchored to the carbonaceous matrix, preventing substantial leaching and ensuring prolonged catalytic activity. Moreover, after five cycles, no significant loss of efficiency was observed, highlighting the enhanced durability of FeOHC-C compared to FeOHC.

Interestingly, by the final reuse cycle, the differences in performance between the two synthesized materials were minimal, suggesting that both composites ultimately reached a steady-state efficiency. Additionally, no detectable degradation byproducts were observed in the aqueous phase after each catalytic cycle, indicating the effectiveness of the heterogeneous Fenton system in mineralizing 2-CP without generating secondary pollutants. This stability and recyclability reinforce the potential of iron oxide/hydrochar composites for sustainable water treatment applications.

Conclusions

Iron oxide/activated hydrochar composites derived from BSG were successfully synthesized through incipient wet impregnation and chemical coprecipitation methods. Characterization of the materials revealed a mesoporous surface with BET surface areas ranging from 44 to 259 m^2/g, indicating a well-developed porous network suitable for adsorption and catalytic applications. XRD analysis confirmed that magnetite (Fe_3O_4) was the predominant iron oxide phase on the carbonaceous surface. The materials demonstrate dual-functionality in water treatment, combining high adsorption capacity with efficient Fenton catalytic activity for 2-CP removal. Adsorption studies showed that the synthesized materials followed the Elovich kinetic model, while the equilibrium data were best described by the Sips isotherm, suggesting monolayer adsorption with slight heterogeneity, with adsorption capacities ranging from 18.70 to 24.63 mg/g. Thermodynamic analysis confirmed that the adsorption process was spontaneous and exothermic, primarily driven by physical interactions, including hydrogen bonding, π–π interactions, and electrostatic attraction between the adsorbent surface and the 2-CP molecules. Heterogeneous Fenton oxidation experiments showed that 2-CP degradation was most efficient under acidic to neutral conditions (pH 3.0–6.0), where the generation of hydroxyl radicals was enhanced due to increased Fe^{2+} availability. Significant loss of efficiency was observed at alkaline pH values. Increasing H_2O_2 concentration improved degradation efficiency, but no further enhancement was observed, likely due to radical scavenging effects. Reusability assays confirmed the long-term stability of the composites. While FeOHC exhibited a decline in efficiency after two cycles due to iron leaching, FeOHC-C maintained consistent removal performance over five cycles, highlighting the stabilizing effect of carbonaceous support on the active catalytic sites.

Overall, these findings demonstrate that iron oxide/hydrochar composites are effective, sustainable, and reusable materials for the remediation of chlorinated organic pollutants in water. Their combined adsorption and catalytic properties, along with their stability under operating conditions, position them as promising candidates for scalable water treatment applications. Future research should explore their performance in more complex water matrices containing competing organic and inorganic species, another activating agent like visible light (Fenton- like reaction), as well as assess their long-term regeneration capacity over extended catalytic cycles to further validate their practical implementation.

Data availability

The datasets used or analyzed during the current study are available from the corresponding author upon reasonable request.

Received: 18 October 2024; Accepted: 24 March 2025
Published online: 28 March 2025

References

1. Lin, R. et al. Synergistic effects of oxidation, coagulation and adsorption in the integrated fenton-based process for wastewater treatment: A review. *J. Environ. Manage.* **306**, 114460 (2022).
2. Kumar, N. S., Shaikh, H. M., Asif, M. & Al-Ghurabi, E. H. Engineered biochar from wood apple shell waste for high-efficient removal of toxic phenolic compounds in wastewater. *Scientific Reports 2021 11:1* 11, 1–17 (2021).
3. Garba, Z. N. et al. An overview of Chlorophenols as contaminants and their removal from wastewater by adsorption: A review. *J. Environ. Manage.* **241**, 59–75 (2019).
4. Adewuyi, A., Göpfert, A., Adewuyi, O. A. & Wolff, T. Adsorption of 2-chlorophenol onto the surface of underutilized seed of adenopus breviflorus: A potential means of treating waste water. *J. Environ. Chem. Eng.* **4**, 664–672 (2016).
5. Garba, Z. N. & Rahim, A. A. Evaluation of optimal activated carbon from an agricultural waste for the removal of para-chlorophenol and 2,4-dichlorophenol. *Process Saf. Environ. Prot.* **102**, 54–63 (2016).
6. Kumakiri, I., Hokstad, J., Peters, T. A., Melbye, A. G. & Ræder, H. Oxidation of aromatic components in water and seawater by a catalytic membrane process. *J. Pet. Sci. Eng.* **79**, 37–44 (2011).
7. Lim, J. W., Lim, P. E., Seng, C. E. & Adnan, R. Simultaneous 4-chlorophenol and nitrogen removal in moving bed sequencing batch reactors packed with polyurethane foam cubes of various sizes. *Bioresour Technol.* **129**, 485–494 (2013).
8. JIANG, Y. et al. Biodegradation of phenol and 4-Chlorophenol by the mutant strain CTM 2. *Chin. J. Chem. Eng.* **16**, 796–800 (2008).
9. Ghaffari, A., Tehrani, M. S., Husain, S. W., Anbia, M. & Azar, P. A. Adsorption of Chlorophenols from aqueous solution over amino-modified ordered nanoporous silica materials. *J. Nanostructure Chem.* **4**, 1–10 (2014).
10. Garba, Z. N. & Rahim, A. A. Optimization of activated carbon Preparation conditions from prosopis Africana seed hulls for the removal of 2,4,6-Trichlorophenol from aqueous solution. *Desalin. Water Treat.* **56**, 2879–2889 (2015).
11. Georgi, A. & Kopinke, F. D. Interaction of adsorption and catalytic reactions in water decontamination processes: part I. Oxidation of organic contaminants with hydrogen peroxide catalyzed by activated carbon. *Appl. Catal. B.* **58**, 9–18 (2005).
12. Daniels, S. V. et al. Synergy of adsorption and Fenton processes in water decontamination: A review. *Sep. Purif. Technol.* **348**, 127803 (2024).
13. Song, J., Zhu, L., Yu, S., Li, G. & Wang, D. The synergistic effect of adsorption and Fenton oxidation for organic pollutants in water remediation: an overview. *RSC Adv.* **14**, 33489–33511 (2024).
14. Wang, C., Liu, H. & Sun, Z. Heterogeneous photo-Fenton reaction catalyzed by nanosized iron oxides for water treatment. *Int. J. Photoenergy* **2012**, 1-10 (2012).
15. Zhou, G. Photocatalytic degradation of organic compounds using carbon based composite catalysts. (2013).
16. Navalon, S., Dhakshinamoorthy, A., Alvaro, M. & Garcia, H. Heterogeneous Fenton catalysts based on activated carbon and related materials. *ChemSusChem* **4**, 1712–1730 (2011).

17. Liang, C. et al. Heterogeneous photo-Fenton degradation of organic pollutants with amorphous Fe-Zn-oxide/hydrochar under visible light irradiation. *Sep. Purif. Technol.* **188**, 105–111 (2017).
18. Yu, S. H. et al. From starch to metal/carbon hybrid nanostructures: hydrothermal Metal-Catalyzed carbonization. *Adv. Mater.* **16**, 1636–1640 (2004).
19. Han, Z. H., Yang, B., Kim, S. H. & Zachariah, M. R. Application of hybrid sphere/carbon nanotube particles in nanofluids. *Nanotechnology* **18**, 105701 (2007).
20. Shende, R. & Sundara, R. Nitrogen doped hybrid carbon based composite dispersed nanofluids as working fluid for low-temperature direct absorption solar collectors. *Sol. Energy Mater. Sol. Cells*. **140**, 9–16 (2015).
21. Ong, Y. T., Ahmad, A. L., Zein, S. H. S. & Tan, S. H. A review on carbon nanotubes in an environmental protection and green engineering perspective. *Braz. J. Chem. Eng.* **27**, 227–242 (2010).
22. Titirici, M. M., Thomas, A., Yu, S. H., Müller, J. O. & Antonietti, M. A direct synthesis of mesoporous carbons with bicontinuous pore morphology from crude plant material by hydrothermal carbonization. *Chem. Mater.* **19**, 4205–4212 (2007).
23. Olszewski, M. P., Nicolae, S. A., Arauzo, P. J., Titirici, M. M. & Kruse, A. Wet and dry? Influence of hydrothermal carbonization on the pyrolysis of spent grains. *J. Clean. Prod.* **260**, 121101 (2020).
24. El Korhani, O. et al. Synthesis and performances of bio-sourced nanostructured carbon membranes elaborated by hydrothermal conversion of beer industry wastes. *Nanoscale Res. Lett. 2013*. **8:1 8**, 1–11 (2013).
25. Anabalón Fuentes, P. et al. Development of bifunctional Biochar/iron oxide composites for Tetracycline removal from synthetic wastewater. *J. Water Process. Eng.* **64**, 105509 (2024).
26. Zhang, X. et al. Hydrochar magnetic adsorbent derived from Chinese medicine industry waste via one-step hydrothermal route: mechanism analyses of magnetism and adsorption. *Fuel* **326**, 125110 (2022).
27. Guel-Nájar, N. A. et al. Magnetic Biochar obtained by chemical coprecipitation and pyrolysis of corn cob residues: characterization and methylene blue adsorption. *Mater. 2023*. **16**, 3127 (2023).
28. Wojciechowska, A., Markowska-Szczupak, A. & Lendzion-Bieluń, Z. TiO2-Modified magnetic nanoparticles (Fe3O4) with antibacterial properties. *Mater. 2022*. **15**, 1863 (2022).
29. de Araújo, T. P., Quesada, H. B., Bergamasco, R., Vareschini, D. T. & de Barros, M. A. S. D. Activated hydrochar produced from Brewer's spent grain and its application in the removal of acetaminophen. *Bioresour Technol.* **310**, 123399 (2020).
30. MacHado, L. M. M. et al. Treatment of effluents containing 2-chlorophenol by adsorption onto chemically and physically activated biochars. *J. Environ. Chem. Eng.* **8**, 104473 (2020).
31. Balogun, A. O., Sotoudehniakarani, F. & McDonald, A. G. Thermo-kinetic, spectroscopic study of Brewer's spent grains and characterisation of their pyrolysis products. *J. Anal. Appl. Pyrol.* **127**, 8–16 (2017).
32. Duan, Z. et al. Magnetic Fe3O4/activated carbon for combined adsorption and Fenton oxidation of 4-chlorophenol. *Carbon N Y*. **167**, 351–363 (2020).
33. Ogungbenro, A. E., Quang, D. V., Al-Ali, K. A., Vega, L. F. & Abu-Zahra, M. R. M. Synthesis and characterization of activated carbon from biomass date seeds for carbon dioxide adsorption. *J. Environ. Chem. Eng.* **8**, 104257 (2020).
34. Liu, J. et al. Thallium separation from wastewater using α-FeOOH@Biochar: efficacy and mechanism. *Sep. Purif. Technol.* **306**, 122532 (2023).
35. Xu, J. et al. Removal of Methyl orange from water by Fenton oxidation of magnetic coconut-clothed Biochar. *RSC Adv.* **12**, 24439–24446 (2022).
36. Bastami, T. R. & Entezari, M. H. Activated carbon from Carrot Dross combined with magnetite nanoparticles for the efficient removal of p-nitrophenol from aqueous solution. *Chem. Eng. J.* **210**, 510–519 (2012).
37. Thommes, M. et al. Physisorption of gases, with special reference to the evaluation of surface area and pore size distribution (IUPAC technical Report). *Pure Appl. Chem.* **87**, 1051–1069 (2015).
38. Schlumberger, C. & Thommes, M. Characterization of hierarchically ordered porous materials by physisorption and mercury Porosimetry—A tutorial review. *Adv. Mater. Interfaces*. **8**, 2002181 (2021).
39. Lorente, A. et al. Sustainable production of solid biofuels and biomaterials by Microwave-Assisted, hydrothermal carbonization (MA-HTC) of brewers' spent grain (BSG). *ACS Sustain. Chem. Eng.* **8**, 18982–18991 (2020).
40. Prabakaran, E., Pillay, K. & Brink, H. Hydrothermal synthesis of magnetic-biochar nanocomposite derived from avocado Peel and its performance as an adsorbent for the removal of methylene blue from wastewater. *Mater. Today Sustain.* **18**, 100123 (2022).
41. Gutiérrez-Sánchez, P. et al. Natural clays as adsorbents for the efficient removal of antibiotic Ciprofloxacin from wastewaters: experimental and theoretical studies using DFT method. *J. Ind. Eng. Chem.* **134**, 137–151 (2024).
42. Zhang, N., Reguyal, F., Praneeth, S. & Sarmah, A. K. A green approach of biochar-supported magnetic nanocomposites from white tea waste: production, characterization and plausible synthesis mechanisms. *Sci. Total Environ.* **886**, 163923 (2023).
43. Juang, R. S. et al. Synthesis of magnetic Fe3O4/activated carbon nanocomposites with high surface area as recoverable adsorbents. *J. Taiwan. Inst. Chem. Eng.* **90**, 51–60 (2018).
44. Krishna Murthy, T. P., Gowrishankar, B. S., Krishna, R. H., Chandraprabha, M. N. & Mathew, B. B. Magnetic modification of coffee husk hydrochar for adsorptive removal of methylene Blue: isotherms, kinetics and thermodynamic studies. *Environ. Chem. Ecotoxicol.* **2**, 205–212 (2020).
45. Sayğılı, G. A. & Sayğılı, H. Fabrication of a magnetic hydrochar composite via an in situ one-pot hydrocarbonization strategy for efficient herbicide removal. *Diam. Relat. Mater.* **128**, 109302 (2022).
46. Cea, M., Seaman, J. C., Jara, A., Mora, M. L. & Diez, M. C. Kinetic and thermodynamic study of Chlorophenol sorption in an allophanic soil. *Chemosphere* **78**, 86–91 (2010).
47. Erto, A., Andreozzi, R., Lancia, A. & Musmarra, D. Factors affecting the adsorption of trichloroethylene onto activated carbons. *Appl. Surf. Sci.* **256**, 5237–5242 (2010).
48. Kumara, N. T. R. N., Hamdan, N., Petra, M. I., Tennakoon, K. U. & Ekanayake, P. Equilibrium Isotherm Studies of Adsorption of Pigments Extracted from Kuduk-kuduk (Melastoma malabathricum L.) Pulp onto TiO2 Nanoparticles. *J Chem* 468975 (2014). (2014).
49. Namasivayam, C. & Kavitha, D. Adsorptive removal of 2-chlorophenol by low-cost Coir pith carbon. *J. Hazard. Mater.* **98**, 257–274 (2003).
50. Allwar, A. Removal of phenol and 2-Chlorophenol by banana bunch activated carbon prepared by Hydrothermally-Assisted KOH activation. *Rasayan J. Chem.* **12**, 598–607 (2019).
51. Sharma, S. et al. Activated carbon adsorbent derived from waste biomass, Croton caudatus for efficient removal of 2-chlorophenol from aqueous solution: kinetics, isotherm, thermodynamics and DFT simulation. *Chem. Eng. Res. Des.* **190**, 777–792 (2023).
52. Strachowski, P. et al. An activation-free route to porous magnetic carbon adsorbents for the removal of phenolic compounds. *New J. Chem.* **43**, 10792–10802 (2019).
53. Hadi, S., Taheri, E., Amin, M. M., Fatehizadeh, A. & Aminabhavi, T. M. Adsorption of 4-chlorophenol by magnetized activated carbon from pomegranate husk using dual stage chemical activation. *Chemosphere* **270**, 128623 (2021).
54. Mishra, S., Yadav, S. S., Rawat, S., Singh, J. & Koduru, J. R. Corn husk derived magnetized activated carbon for the removal of phenol and para-nitrophenol from aqueous solution: interaction mechanism, insights on adsorbent characteristics, and isothermal, kinetic and thermodynamic properties. *J. Environ. Manage.* **246**, 362–373 (2019).
55. Deng, J. et al. Multiwalled carbon nanotubes as adsorbents for removal of herbicide diuron from aqueous solution. *Chem. Eng. J.* **193–194**, 339–347 (2012).

56. Cheng, S., Zeng, X. & Liu, P. One-step synthesis of magnetic N-doped carbon nanotubes derived from waste plastics for effective Cr(VI) removal. *Arab. J. Chem.* **17**, 105956 (2024).
57. Hussain, S., Aneggi, E. & Goi, D. Catalytic activity of metals in heterogeneous Fenton-like oxidation of wastewater contaminants: a review. *Environmental Chemistry Letters 2021 19:3* 19, 2405–2424 (2021).
58. Chu, J. H., Kang, J. K., Park, S. J. & Lee, C. G. Application of magnetic Biochar derived from food waste in heterogeneous sono-Fenton-like process for removal of organic dyes from aqueous solution. *J. Water Process. Eng.* **37**, 101455 (2020).

Acknowledgements

This work was supported by FONDECYT Regular Projects N°1201865, FONDECYT Projects N°1231242.

Author contributions

Kopp, M: Writing – original draft, Assays development, Formal analysis, Conceptualization, Software application to analyze the obtained data and literature revision. Anabalón, P: Writing, literature searching, assays development. Rocha, S: Writing – review & editing Romero-García, J.M.: Writing – review & editing, laboratory supervision. Castro, E.: Writing – review & editing and funding. González, M.E.: Writing – review & editing. Cea, M: Writing – review & editing, Visualization, Validation, Investigation, Formal analysis, Conceptualization.

Declarations

Competing interests

The authors declare no competing interests.

Additional information

Supplementary Information The online version contains supplementary material available at https://doi.org/10.1038/s41598-025-95686-4.

Correspondence and requests for materials should be addressed to M.C.

Reprints and permissions information is available at www.nature.com/reprints.

Publisher's note Springer Nature remains neutral with regard to jurisdictional claims in published maps and institutional affiliations.